JOURNAL OF SPACECRAFT AND ROCKETS
Vol. 34, No. 5, September–October 1997

Flow Confluence Past a Jet-On Axisymmetric Afterbody

Philippe Reijasse,* Bernard Corbel,† and Jean Délery‡
ONERA, Châtillon 92322, France

A basic experimental study of the confluence of two turbulent supersonic flows has been carried out in a Mach 2 research wind tunnel. The aim of this investigation was to reach a better understanding of the fluid dynamics mechanisms involved in a typical powered afterbody configuration when an underexpanded nozzle jet interacts with an external flowfield. The experimental techniques used to investigate this flow were wall pressure measurements, schlieren photography, and two-component laser Doppler velocimetry. The mean and fluctuating properties of the flowfield were measured around a jet-on axisymmetric afterbody model. In particular, the results illustrate the effect of the jet-to-external stagnation pressure ratio and give information on the turbulent field. These experiments compensate for the lack of published detailed measurements in such flowfield patterns and provide well-documented test cases to validate computer codes.

Nomenclature

D	= model maximum diameter, mm
k	= turbulent kinetic energy, m^2/s^2
M_e	= outer flow upstream Mach number
p_{te}	= outer flow stagnation pressure, Pa
p_{tj}	= jet stagnation pressure, Pa
T_{te}	= external stagnation temperature, K
T_{tj}	= jet stagnation temperature, K
u, w	= instantaneous streamwise and radial velocity components, m/s
u_∞	= upstream reference velocity, m/s
u', w'	= fluctuating streamwise and radial velocity components, m/s
$\overline{u'^2}$, $\overline{w'^2}$, $\overline{u'w'}$	= Reynolds stress tensor components, m^2/s^2
X, Z	= coordinate axes, defined in Fig. 2
δ_0	= incoming boundary layer thickness, mm
σ_u/u_∞	= normalized streamwise turbulence intensity, where σ_u is $\sqrt{(u'^2)}$
σ_w/u_∞	= normalized radial turbulence intensity, where σ_w is $\sqrt{(w'^2)}$

Introduction

FLOW confluence induces phenomena playing an important role in a large number of applications, notably at the trailing edge of an airfoil or a turbine blade, at the end of a nacelle strut or a fuel injector, and at the base of a projectile. Downstream from the afterbody of powered aerospace vehicles, the confluence process assumes a particular importance because of the different nature of the propulsive jets and external stream. In general, the coflowing streams are nonadapted, which generates, in the supersonic or hypersonic regimes, shock waves interacting with the dissipative layers. When the flows are far from the adaptation state, the strength of the interaction shock can be so severe that it forces boundary-layer separation, either inside an overexpanded nozzle, or on a boat tail because of jet pluming. Boundary-layer separation entails the formation of mixing layers feeding weak dynamic pressure separated zones. Inside these separated regions, the recirculating flow rolls up into well-organized vortical structures, if we consider the time-averaged flow properties. In fact, the instantaneous properties of such recirculating flowfields are fluctuating and characterized by the presence of differently sized and randomly organized eddies. These highly turbulent separated zones, in which eddies ensure effective mixing between the species of the two coflowing dissipative layers, are the seat of complex aerothermochemical processes. Nonadaptation and turbulent transfer phenomena generated by flow confluence have an influence 1) on the intrinsic properties of the propulsive jet that govern, for example, its infrared signature; 2) on the afterbody drag/thrust balance by modifying the pressure distribution on the rear surfaces; 3) on the stability and maneuverability of a missile at a high flight altitude when jet pluming induces an unstable separation of the external flow; 4) on the base heat flux levels, resulting from the combination of gas confinement and the recirculation mechanisms in the base region; and 5) on the thrust of new types of nozzles, especially those applied to the next generation of rocket motors or future supersonic vehicles, for which confluence generates separation inside the nozzle.

Previous experimental studies[1–5] about flow confluence used means of investigation that allowed local quantitative measurements (as the base pressure), or qualitative flow visualizations (as schlieren photography), or the probing of mean flow properties (as pitot pressure). Concurrently, the flow confluence, when it generates extended separated zones, was theoretically treated by the so-called multicomponent approach.[6–9] This semiempirical method, originated from the Korst[6] theory and based on a reattachment criterion, could predict the general thermodynamic properties of the flows. However, the rough hypotheses concerning the turbulent transfer processes did not allow calculation of the pressure inside the separated region with deviations of less than 10–15%, from experimentally measured values. Nevertheless, this theoretical approach is still used today by industry for design purposes because of its very low cost.

Currently, Reynolds-averaged Navier–Stokes computational fluid dynamics codes can predict the mean and the turbulent properties of complex flowfields,[10–11] which necessitates extensive validation presently allowed by the laser Doppler velocimetry (LDV) technique.[12–14] Previous experimental investigations performed at ONERA by using LDV for the study of flow confluence behind jet-on afterbodies started at the beginning of the 1980s. The first study[15] was relative to the flow past an axisymmetric model of a typical tactical missile at Mach 0.85; the second[16] was for the mean recirculating flow past a multinozzle afterbody at Mach 4. In parallel, substantial work has been done by other investigators on the turbulent mixing between planar supersonic streams.[17–20] Also, the case of supersonic axisymmetric coflowing jets has been investigated.[21] These experiments, in which the two flows were nearly adapted, focused on the effect of compressibility on turbulence development in basic situations. However, experimental data relative to the confluence between an outer supersonic flow and a propulsive jet in a more realistic situation and with consideration of the effect on the afterbody aerodynamics are scarce, especially for an aerospike type configuration.

Presented as Paper 96-2449 at the AIAA 14th Applied Aerodynamics Conference, New Orleans, LA, June 17–20, 1996; received July 29, 1996; revision received June 5, 1997; accepted for publication June 5, 1997.

*Head, Aerothermal Problems Group, Experimental/Fundamental Aerodynamics Branch. Member AIAA.
†Technical Engineer, Experimental/Fundamental Aerodynamics Branch.
‡Head, Experimental/Fundamental Aerodynamics Branch. Member AIAA.

For these reasons and in the framework of a research program on a new propulsion system, a fundamental investigation of the aerodynamics of confluence was undertaken, whose main purpose was to provide a detailed experimental analysis of the mean and turbulent properties of two coflowing supersonic streams. These basic experiments[22,23] were performed on axisymmetric models representing the propulsive afterbody of a future supersonic aircraft. For the experiment, 12 model geometries were tested with three nozzle pressure ratios each. Among these 36 test configurations, 5 were investigated by LDV. In the context of this article, 2 LDV-measured configurations are presented, relative to two jet-to-external pressure ratios tested on the same model.

Test Setup and Equipment

A photograph of the model setup in the test section of the continuous Mach 2 wind tunnel is shown in Fig. 1. Desiccated atmospheric air feeds the wind tunnel due to an aspiration plant located downstream of the test section. During the present tests, the stagnation pressure p_{te} and the stagnation temperature T_{te} were close to $0.99 \pm 0.0005 \times 10^5$ Pa and 297 ± 5 K, respectively. The 120×120 mm^2 test section was equipped with a two-dimensional nozzle designed to give a uniform Mach number close to 1.95, without the presence of a central sting. The axisymmetric afterbody model is mounted at the end of the 40-mm-diam central sting, which is fixed upstream of the wind-tunnel nozzle throat. The diameter of the model is also equal to $D = 40$ mm. This kind of arrangement frequently has been used in the past, the perturbations created by the central sting, which is aligned with the main stream, being small, provided that the sting diameter is not too large and that the outer flow Mach number is moderate (less than 3, approximately). At a higher Mach number, it is necessary to use an axisymmetric arrangement with a nozzle whose contour is computed by taking into consideration the presence of the central sting. The model surface was covered with a black paint to reduce laser beam reflection.

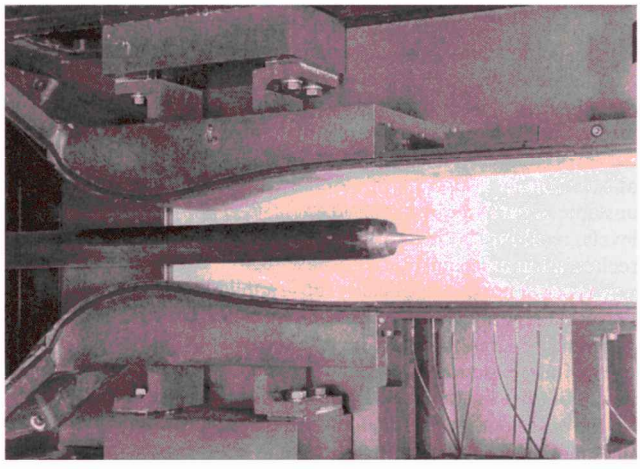

Fig. 1 Afterbody model in the Mach 2 wind tunnel.

The model (Fig. 2) consists of a central plug nozzle mounted inside a hollow cylinder. The cylinder is ended by a boat tail and a small base. The profile of the boat tail is determined by an 804-mm-radius circular arc with an origin located 15.5 mm upstream the base. The annular base surface is delimited by two circles of diameters 37 and 32 mm. The plug spike emerges 56.5 mm off the base plane. The diameter of the plug, in the throat plane located 20 mm upstream of the base, is 20.44 mm. The contour of the annular plug nozzle has been calculated by the method of characteristics to give, in the theoretical case of an adapted jet, a uniform flow with a Mach number equal to 2 in the section at the end of the spike. The plug nozzle was fed by desiccated air at room temperature. The jet stagnation pressure varied from 3 to $5 \pm 0.05 \times 10^5$ Pa, with results presented later for these two extreme values.

A stagnation probe located 600 mm upstream of the wind-tunnel nozzle throat measured the pressure in the plenum chamber. Figure 2 gives the locations of the 28, 0.4-mm-diam static pressure taps equipping the model. Along the cylindrical afterbody and boat tail on the same generating line there are 15 distributed, and there are 6 around the boat tail, 4 on the base located at various circumferential positions on the same radius, and 3 on the plug nozzle. The stagnation and wall pressures were measured with a Statham 15-psia transducer mounted in a Scanivalve. The stabilization of the pressure needed a 15-s scanning time per tap.

The flowfield density variation has been visualized by the schlieren photography technique using a horizontal knife edge. Spark schlieren photographs have been obtained with a Nanolite light source, allowing a 20-ns exposure time.

The LDV system has been used in its two-component version; the three-component capability has not been employed for this axisymmetric flow investigation. The light source is a 15-W argon ion laser operating at 8 W for all lines. The crossing of

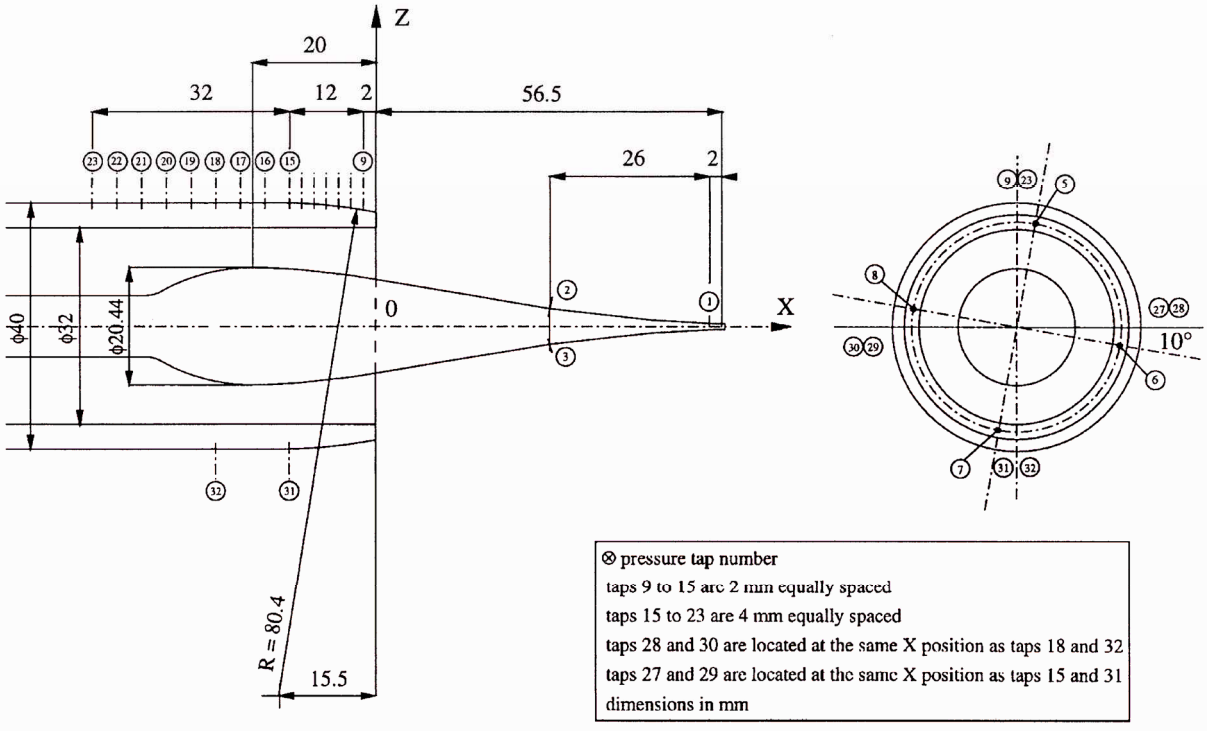

Fig. 2 Model geometrical definition.

semitransparent mirrors allows selection of the green and blue lines, with their wavelengths 514.5 and 488.0 nm, respectively. Each beam is divided when it crosses beam splitters. The two resulting monochromatic beams are then focused to create an interference fringe pattern. The diameter of the probe volume, constituted by the two fringe systems, is 200 μm, and the focal distance is 1 m. The blue and green fringe spacings are 13.165 and 12.684 μm, respectively. Frequency shifting at 15 MHz is used to discriminate the direction of the measured velocity component. The beam pairs are oriented at ± 45 deg to the streamwise direction. The LDV system worked in the forward scatter mode. The collecting optics consist of a Cassegrain telescope, which collects the light scattered by the particles crossing the measurement volume. The scattered light is converted into an analog voltage signal by photomultipliers; this analog signal then feeds DANTEC type 55L counters. An interface simultaneity criterion ensures that the data from the two channels are relative to the same particle. The external stream is seeded with sprayed olive oil by means of a movable tube placed in the wind-tunnel plenum chamber. The seeding of the jet is ensured by submicron (0.5 μm diam) silicon dioxide (SiO_2) particles injected far upstream of the model nozzle throat.

The relative accuracies of experimental data are 1% for the pressure measurements, 1% of the upstream outer flow velocity magnitude for the mean velocity components, and 8 and 10% for the normal stress and the turbulent shear stress components, respectively.

Results and Discussion

Flowfield Visualizations

The spark schlieren photographs (Figs. 3a and 3b) give the main features of the afterbody flowfields obtained for the two nozzle pressure ratios $p_{tj}/p_{te} = 3.03$ and 5.05, respectively. In both cases, these visualizations indicate a shock produced by the separation of the external boundary layer developing on the boat tail. This separation shock meets a second shock, crossing the external flow, which is due to the confluence of the flows. We see the reflection of the confluence shock on the top and bottom walls of the test section, and we can also distinguish slight traces of the reflection process on the glass side windows of the wind tunnel. We can notice that this reflected shock does not interact with the confluence region. The same observation can be made for the waves forming at the junction between the wind-tunnel nozzle blocks and the top and bottom rectilinear walls of the test section.

After flow separation, occurring near the end of the boat tail for the external stream and near the nozzle lip for the jet, the flow boundaries envelop a separated region before coflowing. The confluence process starts the development of a wake, which ensures the mutual adaptation of the flows. In the nozzle exit region, we distinguish an expansion fan centered near the nozzle lip. The expansion is followed by a wave focalization process, which creates the classical barrel shock structure of an underexpanded jet, clearly visible in Figs. 3a and 3b. The reflection of the barrel shock at the centerline is slightly perturbed by test section unstarting effects, which begin in the symmetry axis zone. This partial unstarting occurs far enough downstream of the plug nozzle, so that this effect does not influence the flowfield characteristics around the afterbody model, in particular, in the confluence region. In summary, these photographs clearly show a shock-wave/boundary-layer interaction induced by the jet pluming, the strongly underexpanded jet behaving as a fluid ramp facing the external flow.

By comparing Figs. 3a and 3b, we can see the effects due to the increase of the nozzle pressure ratio on the flowfield pattern: in particular, the accentuation of the jet pluming with the widening of the barrel shock, the augmentation of the fluid ramp angle, the raising of the external confluence shock intensity, and a more upstream interaction on the boat tail.

Pressure Measurements

Figures 4a and 4b present the wall pressure distributions measured on the boat tail and normalized by the upstream static pressure p_∞. The two series of four pressure taps each located on a circumferential line around the boat tail at the streamwise stations $X = -14$ and -26 mm indicate good symmetry of the upstream flow.

The aspect of the pressure distribution on the same generating line is typical of an interaction between the external boundary layer and a shock, as we could see in the schlieren photographs. At first, the approach static pressure ratio p_e/p_∞ on the cylindrical part of the model is nearly constant and close to 1. The flow expansion induced by the boat tail makes the static pressure decrease. Then, at a certain location X_0, close to -6 mm for $p_{tj}/p_{te} = 3.03$ and between -6 and -10 mm for $p_{tj}/p_{te} = 5.05$, the pressure goes up rapidly when the boundary layer crosses a narrow compression wave system located at the foot of the separation shock. This rapid pressure rise is noticed on the final part of the boat tail up to the last pressure tap p_9, located 2 mm before the base edge (see Fig. 2).

Table 1 gives the base pressure compared with the pressure p_9 on the boat tail. For each jet-to-external pressure ratio, a maximum difference of 5% between the four base pressure values confirms the fairly good circumferential symmetry of the flowfield. The base pressures are higher (about 17 and 5% for $p_{tj}/p_{te} = 3.03$ and 5.05, respectively) than the wall pressure p_9. The Mach number of the jet at the nozzle exit was equal to 2.59 for $p_{tj}/p_{te} = 3.03$ and to 2.85 for $p_{tj}/p_{te} = 5.05$.

Table 1 Base pressure compared with the boat tail pressure

Pressure tap location	Pressure tap no.	p/p_∞	
		$p_{tj}/p_{te} = 3.03$	$p_{tj}/p_{te} = 5.05$
Base	5	1.180	1.318
Base	6	1.242	1.377
Base	7	1.184	1.339
Base	8	1.232	1.358
Base	Mean value	1.2095	1.348
Boat tail	9	1.028	1.290

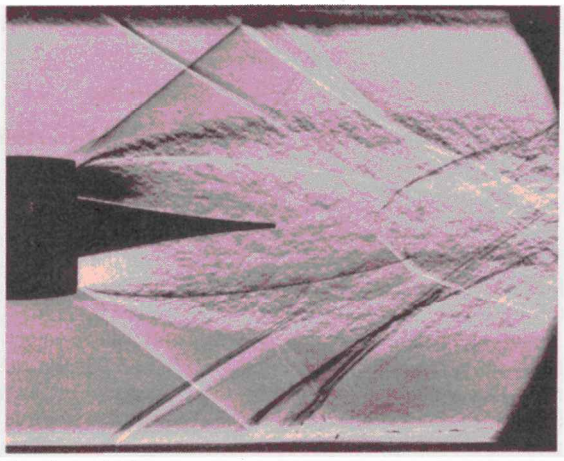

a) $p_{tj}/p_{te} = 3.03$

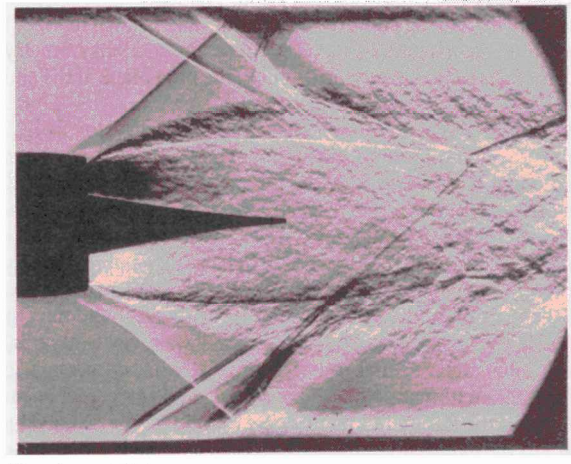

b) $p_{tj}/p_{te} = 5.05$

Fig. 3 Spark schlieren photographs of the flowfield.

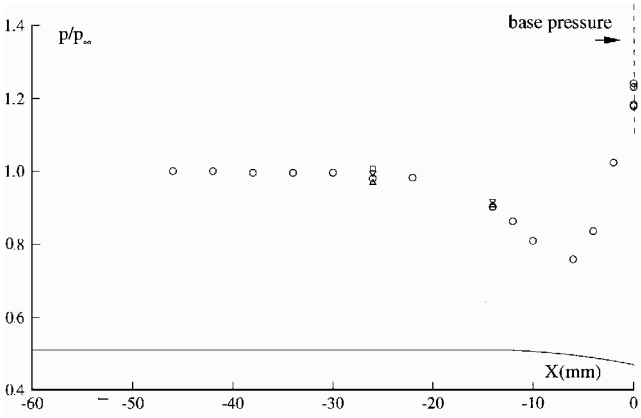

a) $p_{tj}/p_{te} = 3.03$

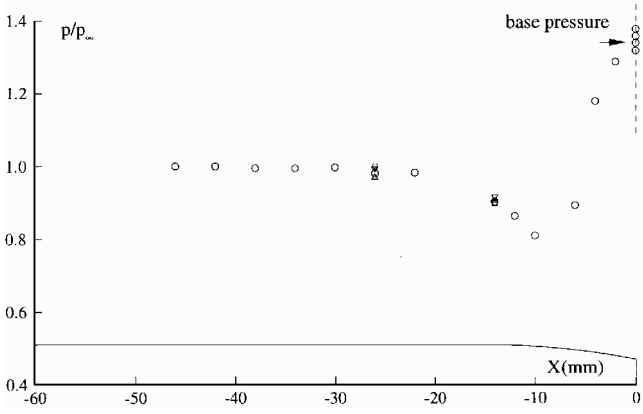

b) $p_{tj}/p_{te} = 5.05$

Fig. 4 Surface pressure distributions on the afterbody.

In a typical two-dimensional shock-wave/turbulent boundary-layer interaction with an extended separated zone,[24] the effective separation is followed by a plateau pressure region. As this plateau region is generally observed a little downstream of the pressure rise, we can say that, in the case of $p_{tj}/p_{te} = 3.03$, no effective separation occurs on the boat tail. Such a case, when the pressure rise is not strong enough to induce effective separation, is called incipient separation. On the other hand, in the configuration $p_{tj}/p_{te} = 5.05$, the 5% difference between the base pressure and the boat tail value makes the onset of an effective separation much more probable.

LDV Measurements

For each configuration, about 2300 measurement points have been recorded, which are distributed over 40 axial stations: 11 on the boat tail, 19 on the spike, and the remaining ones downstream of the spike. In general, 2000 values of the instantaneous velocity were recorded for each measurement point. The LDV measurement stations are defined in the coordinate system OXZ (shown in Fig. 2) that consists of the streamwise axis X along the model symmetry axis and the radial axis Z with the origin in the base plane at the end of the boat tail.

The streamwise mean component of the external velocity u_∞, in the uniform flow region at the station $X/D = -0.1$, has been measured equal to 519 and 512 m/s for $p_{tj}/p_{te} = 3.03$ and 5.05, respectively. Considering the respective external stagnation temperatures (302 and 297 K), the mean freestream Mach number was equal to 1.998 and 1.981, respectively. These values are slightly higher than the nozzle design Mach number because of the presence of the central sting. The resulting unit Reynolds number is equal to $12.24 \times 10^6\ \mathrm{m}^{-1}$. Subsequently, the streamwise and radial turbulence intensities, σ_u and σ_w, respectively, will be normalized by the upstream external velocity u_∞, whereas the turbulent shear stress $\overline{u'w'}$ and the turbulent kinetic energy k will be normalized by the square of the external velocity u_∞^2. The circumferential velocity component v not being measured, the turbulent kinetic energy k has been estimated by the following formula:

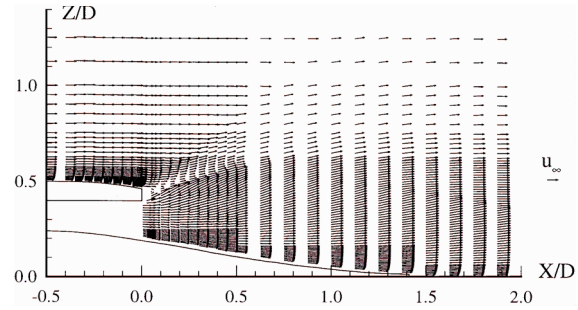

a) $p_{tj}/p_{te} = 3.03$

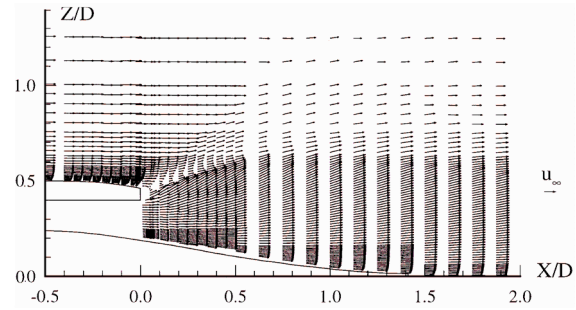

b) $p_{tj}/p_{te} = 5.05$

Fig. 5 General views of the mean velocity vector field.

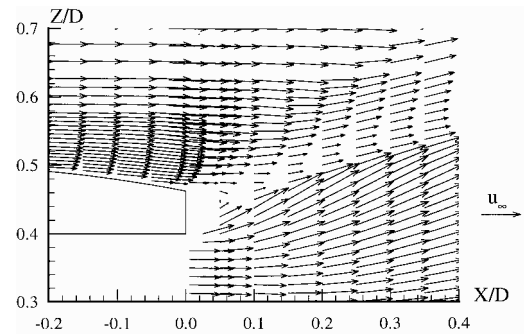

a) $p_{tj}/p_{te} = 3.03$

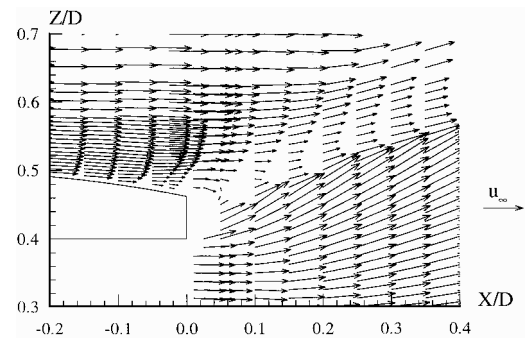

b) $p_{tj}/p_{te} = 5.05$

Fig. 6 Enlarged views of the mean velocity vector field.

$$k = \tfrac{1}{2}\left[\overline{u'^2} + \overline{w'^2} + \tfrac{1}{2}(\overline{u'^2} + \overline{w'^2})\right] = \tfrac{3}{4}(\overline{u'^2} + \overline{w'^2})$$

According to LDV measurements made in the freestream outer flow, at stations $X/D = -1$ and -0.5, the approach boundary-layer thickness δ_0 can be evaluated to be about 7.1 ± 0.1 mm.

Figures 5a and 5b give general views of the mean velocity vector fields for $p_{tj}/p_{te} = 3.03$ and for $p_{tj}/p_{te} = 5.05$. We can see the main flow deviations induced by the crossing of either the outer confluence shock or the barrel shock. We can also observe the progressive mutual adaptation of the coflowing streams along a wake region. Figures 6a and 6b give enlarged views of the boat tail region in which we can see the outer flow expansion and the initial

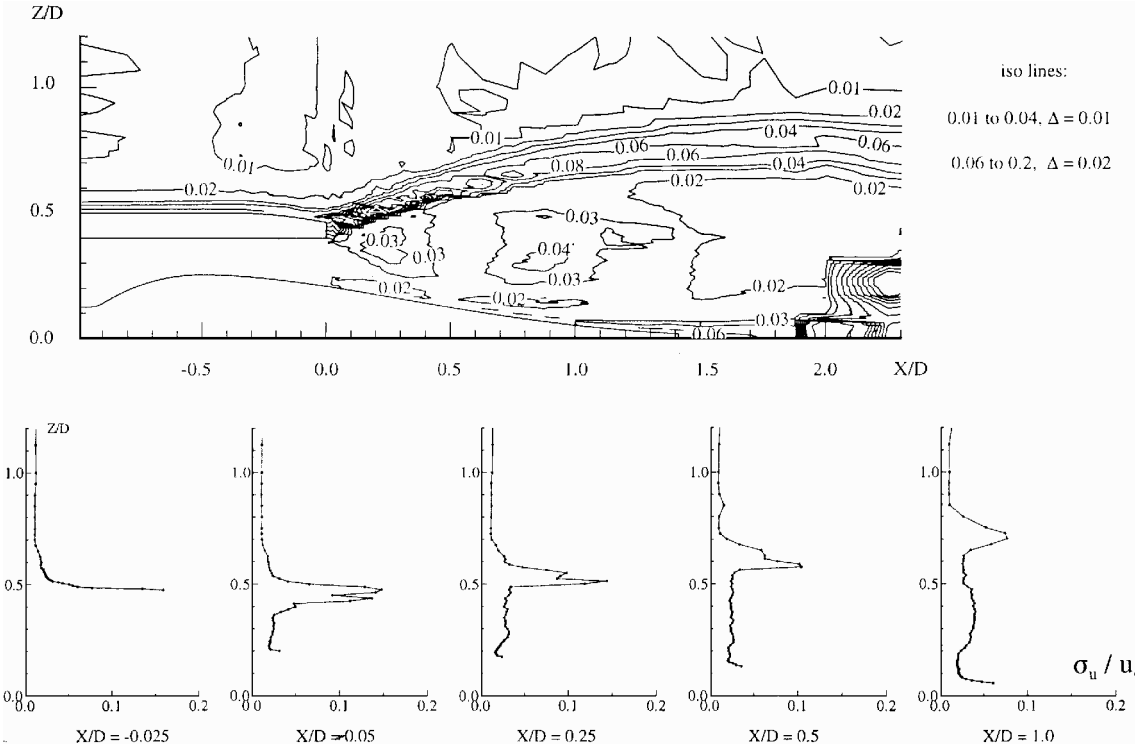

a) Case p_{tj}/p_{te} = 3.03

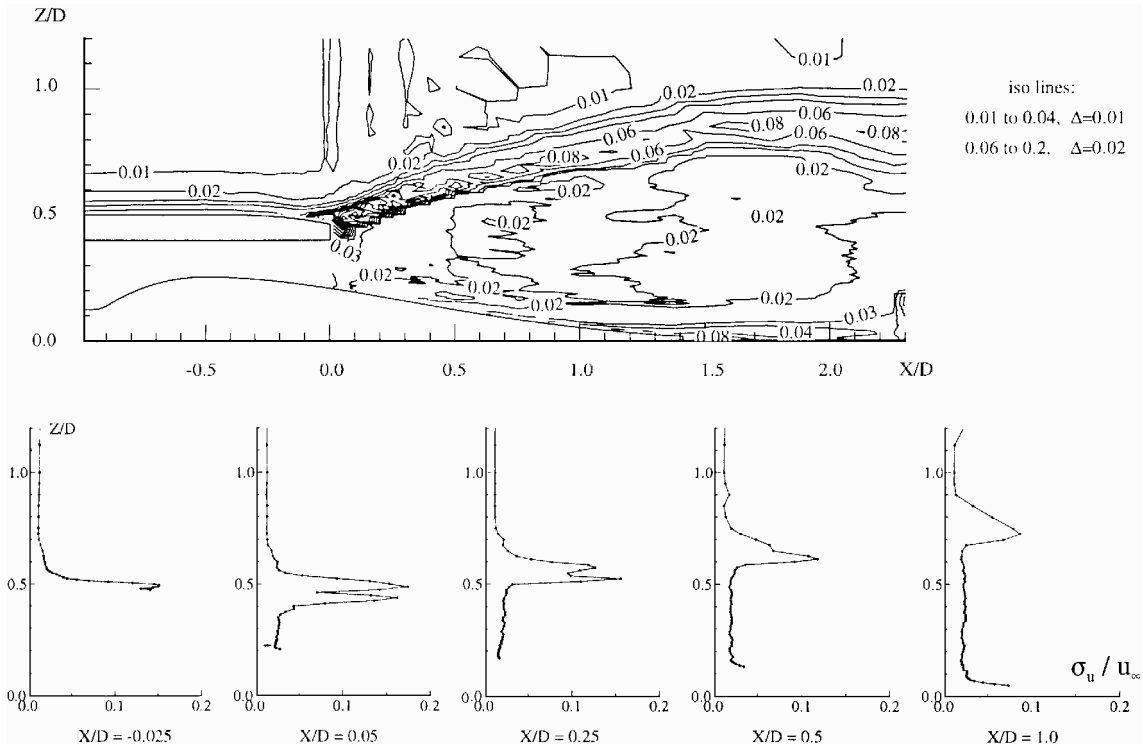

b) Case p_{tj}/p_{te} = 5.05

Fig. 7 Streamwise turbulence intensity σ_u/u_∞.

development of the mixing layers. No measurement point could be recorded very near the base surface because of the scarcity of seeding particles in this separated region. The nearest station to the base, which is completely measured, is located at $X = 2$ mm or $X/D = 0.05$. At this station, we can see that the streamwise component of the mean velocity becomes nearly equal to zero or can even be negative, especially when $p_{tj}/p_{te} = 5.05$. Although no measurement data were obtained just behind the base, we can guess the trend of flow recirculation toward the base. Deduced from LDV measurements, the convective Mach number at the end of the confluence region was close to 0.2 for the two expansion ratios. This low value results from the fact that the velocities in the jet and outer flow differ only by about 100 m/s, the sound speeds in the two streams being nearly equal. In these conditions, we cannot expect significant compressibility effects in the development of the shear layer separating the jet and the outer flow.

In the freestream outer flow, the level of the streamwise turbulence intensity σ_u/u_∞ is equal to 0.01 ± 0.001, as we can see in Figs. 7a and 7b. In fact, this turbulence level is the lowest value measurable with the LDV system under the present conditions because of

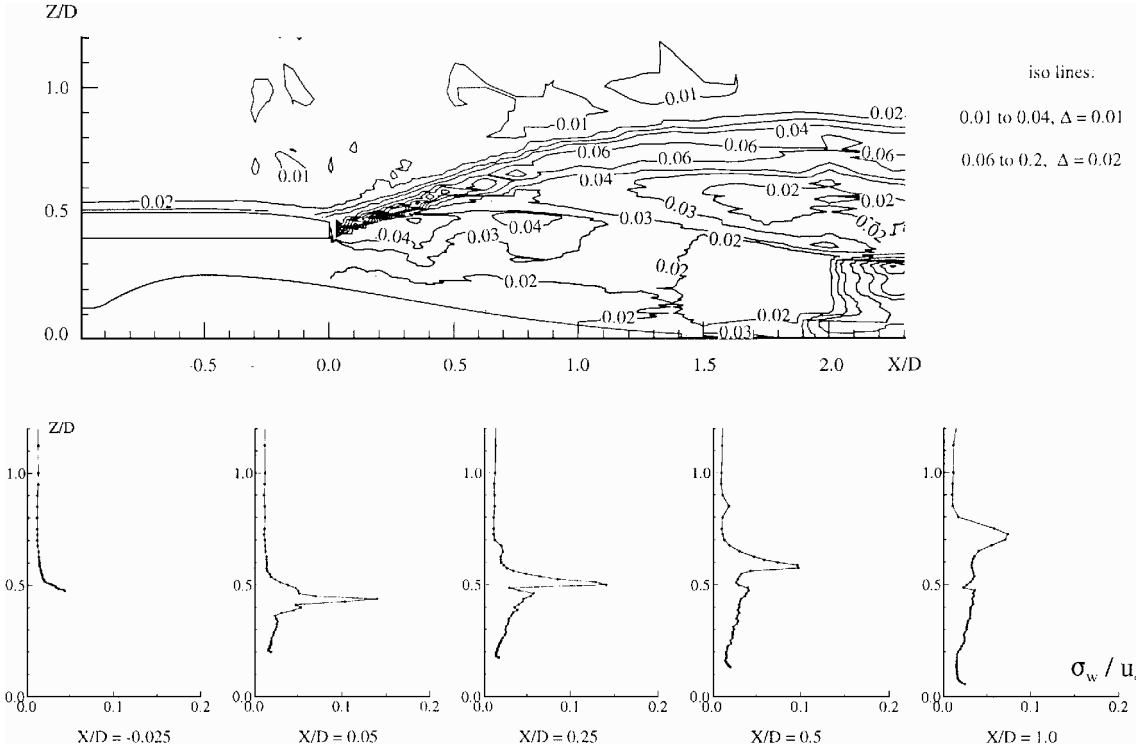

a) Case p_{tj}/p_{te} = 3.03

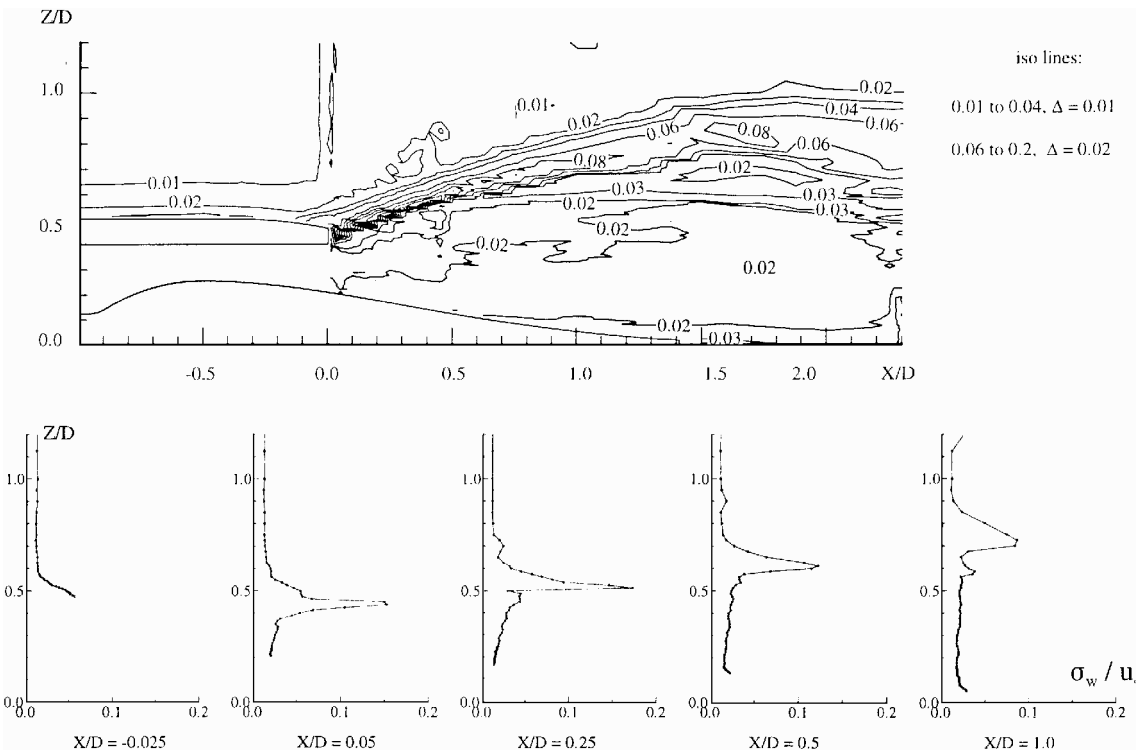

b) Case p_{tj}/p_{te} = 5.05

Fig. 8 Radial turbulence intensity σ_w/u_∞.

measurement uncertainties. The true turbulence intensity in the outer stream is probably lower. Inside the boundary layers developing along the boat tail and the plug nozzle, we observe the rapid growth of σ_u/u_∞. The streamwise turbulent intensity increases much more when the shock/boundary-layer interaction is at its onset (see station $X/D = -0.025$). The σ_u levels remain high in the mixing layers all along the confluence process. Each shear layer shows a maximum value of σ_u near its center (see stations $X/D = 0.05$ and 0.25). Then, at station $X/D = 0.5$ and after, dissipative phenomena become more important (and turbulence production is reduced), and the wake region is characterized by only one maximum value decreasing steadily as we go farther downstream.

By comparing Figs. 7a and 7b, we can see that raising the jet-to-external stagnation pressure ratio from 3.03 to 5.05 augments the maximum levels of streamwise turbulence intensity σ_u by about 10–15% inside the wake region. This is due to the increased shear in the wake for the more highly underexpanded jet. In the nozzle exit region, the σ_u levels are near 0.02 for the two cases $p_{tj}/p_{te} = 3.03$ and 5.05. But farther downstream of the nozzle exit, we can notice that the σ_u levels go up to 0.04 in the case $p_{tj}/p_{te} = 3.03$, whereas

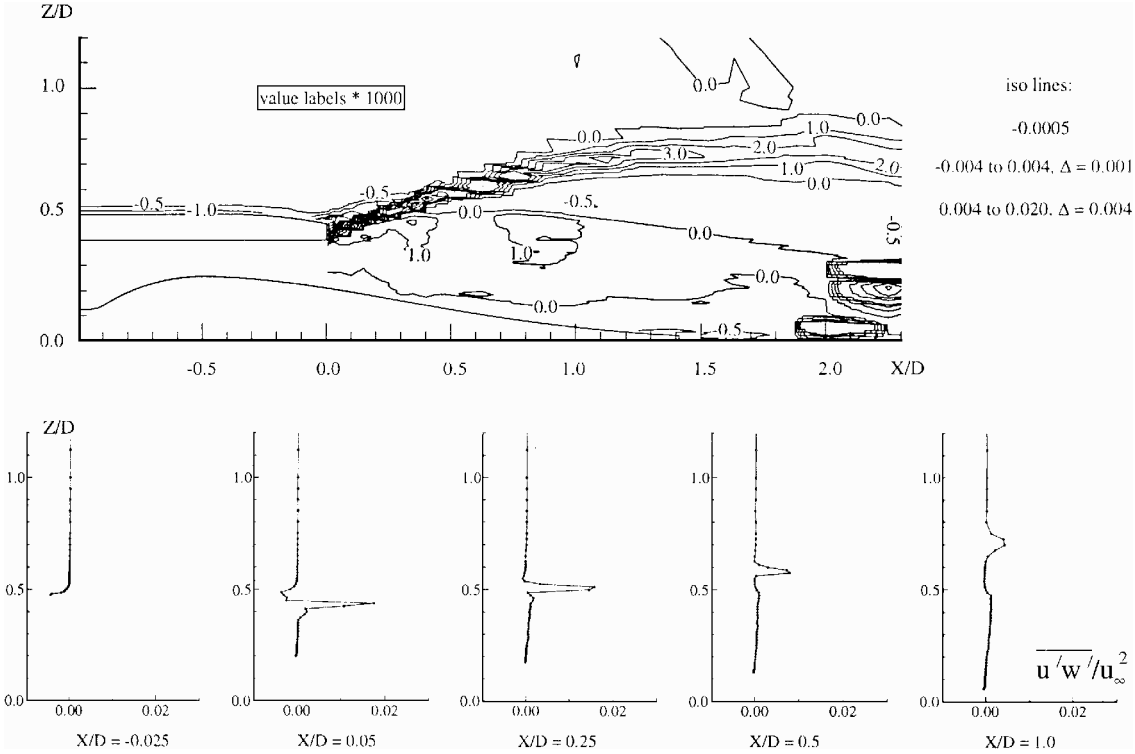

a) Case p_{tj}/p_{te} = 3.03

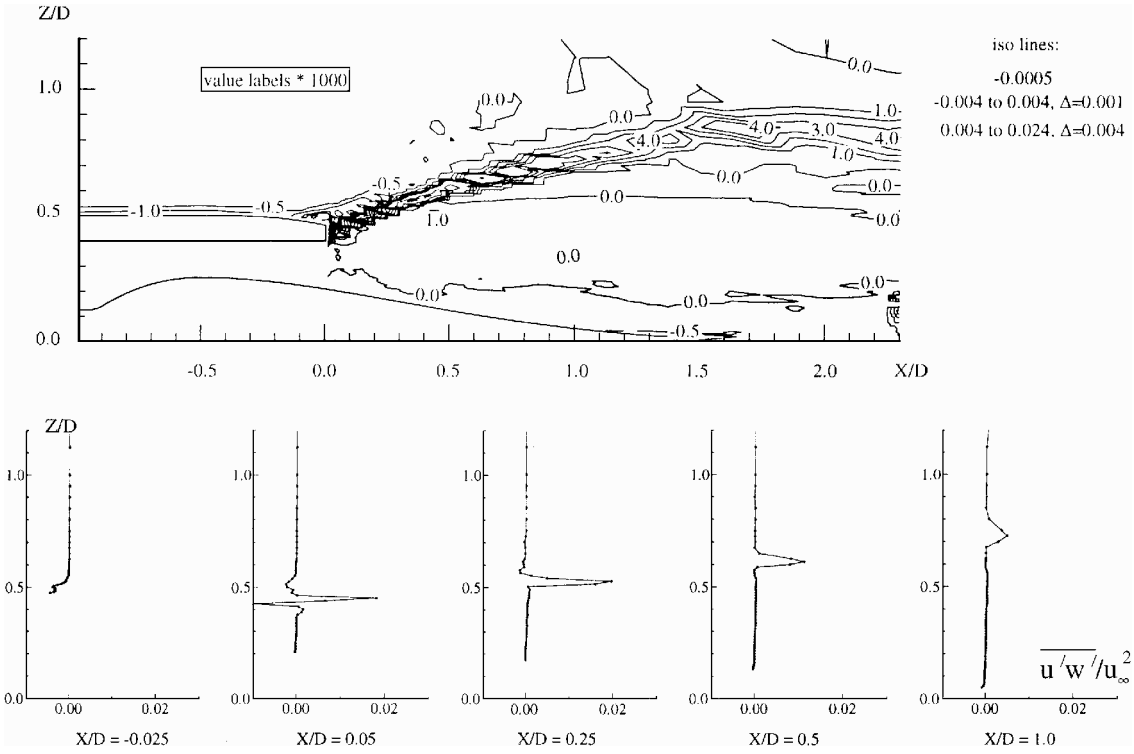

b) Case p_{tj}/p_{te} = 5.05

Fig. 9 Turbulent shear stress $\overline{u'w'}$.

they remain constant and close to 0.02 in the case $p_{tj}/p_{te} = 5.05$. There is no clear explanation of the relatively high turbulence levels found in the central part of the jet where the flow should be inviscid. These levels are either due to increased measurement uncertainties or reflect the turbulence of the boundary layer developing in the upstream long supply pipe.

Figures 8a and 8b give the levels of the radial turbulence intensity σ_w. In the freestream outer flow, the radial component σ_w has about the same level as the streamwise component σ_u. At station $X/D = 0.05$ and after, the maximum values of σ_w become important but only inside the propulsive jet shear layer. Downstream of the nozzle exit, the radial component σ_w seems much more influenced by the expansion process and by the wave focusing process than the streamwise component. Contrary to σ_u, we can notice, at the barrel shock location, a significant increase of the radial turbulence intensity σ_w. Concerning the influence of the jet-to-external pressure ratio on the σ_w levels, we can make the same remarks as made previously for the streamwise component σ_u.

The levels of the turbulent shear stress $\overline{u'w'}$ and the turbulent kinetic energy k are close to zero in the inviscid flow regions, as we

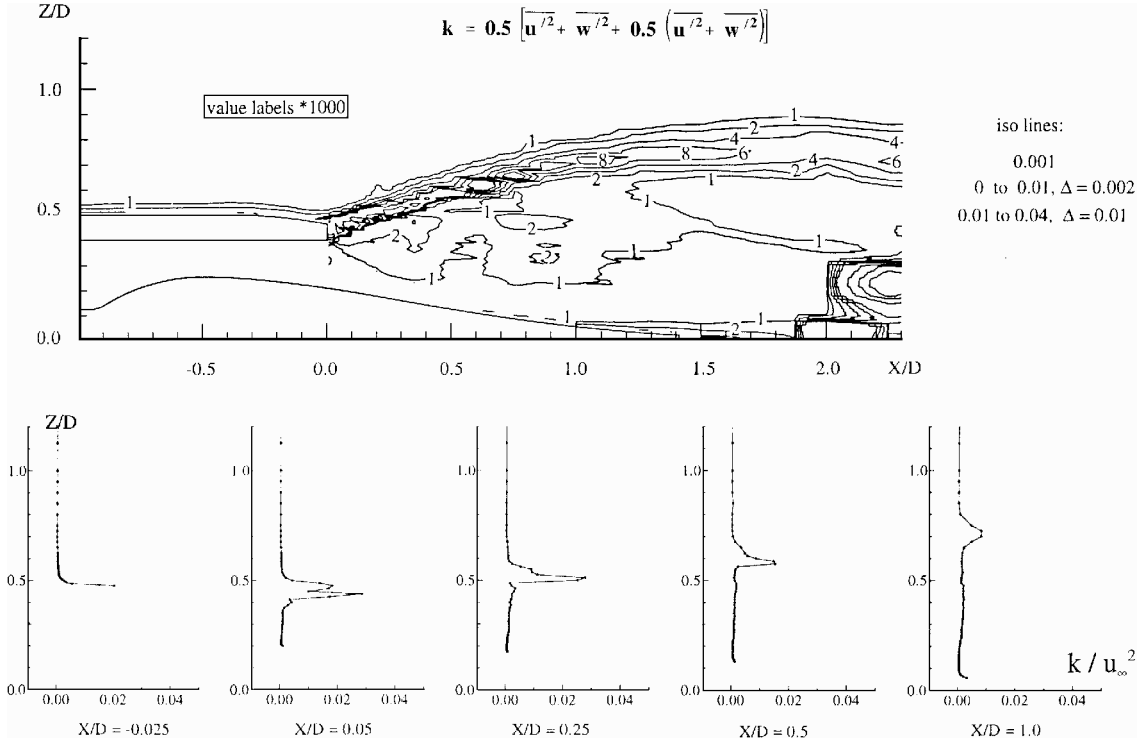

a) Case p_{tj}/p_{te} = 3.03

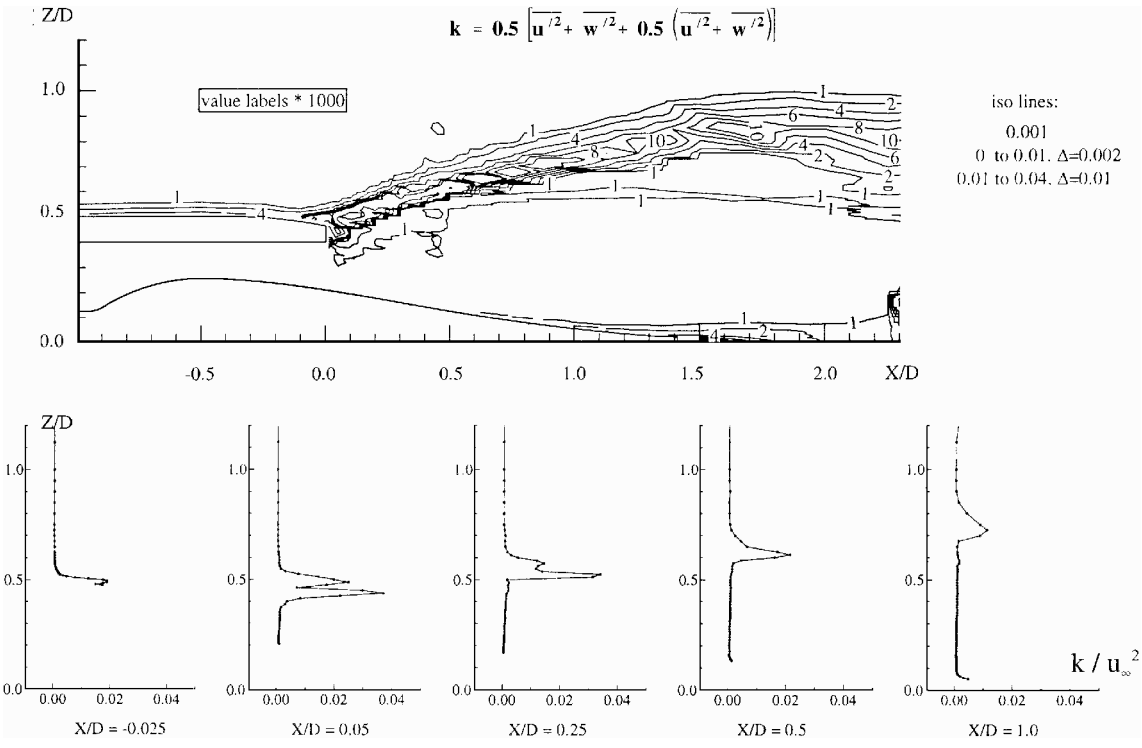

b) Case p_{tj}/p_{te} = 5.05

Fig. 10 Turbulence kinetic energy k/u^2_∞.

can see in Figs. 9 and 10. They begin to rise in the outer boundary layer and in the mixing layers. Because of large structures in shear layer, the values of $\overline{u'w'}$ and k are far more important in the propulsive jet shear layer than in the outer flow. High levels of $\overline{u'w'}$ and k are maintained in the jet dissipative layer all along the confluence process, as we can see at stations $X/D = 0.05$ and 0.25. Then, $\overline{u'w'}$ and k decrease as the wake develops farther downstream, again due to the reduced turbulence production. In the wake region, we can see that the increase of the jet-to-external stagnation pressure ratio induces a small rise of the shear stress levels, and it makes the turbulent kinetic energy increase, more significantly, by about 20–40%. Downstream from the nozzle exit, in the jet flow, a small increase of $\overline{u'w'}$ and k can be seen when $p_{tj}/p_{te} = 3.03$, whereas these levels remain relatively constant and close to zero when $p_{tj}/p_{te} = 5.05$.

Conclusion

These basic experiments have allowed a detailed investigation of the confluence between two turbulent supersonic flows past a jet-on axisymmetric afterbody. The measurements have revealed that,

on the boat tail surface, typical shock-wave/boundary-layer interactions and separations occur induced by the jet pluming, the underexpanded jet behaving as a fluid ramp facing the external flow. If we can conclude that an effective separation of the external boundary layer occurs for the highest nozzle pressure ratio, it is only an incipient separation that occurs for the smallest one.

The LDV measurements have given information on the mean flow properties and turbulent characteristics of this afterbody flowfield. The highest turbulence levels are located in the separated shear layers, all along the confluence region. These levels decrease but remain important going farther downstream in the wake. The rise of the nozzle pressure ratio (p_{tj}/p_{te} from 3.03 to 5.05) induces a 10–15% increase of the turbulence levels in the wake region but a significant decrease of these levels in the jet expansion region downstream of the nozzle exit. Complex turbulent processes occur in supersonic flow confluence and may have an important role on the thrust balance of propulsive afterbodies. Therefore, in such strongly compressible flows (containing shock waves, expansion fans, and separated regions), turbulence modeling remains a challenge. The present experimental results compensate for the lack of published detailed measurements for this type of flow, and they contribute to provide well-documented test cases for the validation of computer codes.

Acknowledgments

The present study has been executed under contract from the Direction des Recherches et Etudes Techniques of the French Ministry of Defense. The laser Doppler velocimetry measurements were performed by the laser velocimetry group of the Experimental/Fundamental Aerodynamics Branch of ONERA. The authors are very grateful to the reviewer for his valuable corrections and suggestions.

References

[1]Reid, J., and Hastings, R. C., "The Effect of a Central Jet on the Base Pressure of a Cylindrical Afterbody in a Supersonic Stream," Aeronautical Research Council, Rept. ARC R&M 3224, Dec. 1959.

[2]Carrière, P., and Sirieix, M., "Effets aérodynamiques de l'éclatement d'un jet de fusée (Aerodynamic Effect of Jet Pluming)," *La Recherche Aéronautique*, No. 89, July–Aug. 1962, pp. 3–10.

[3]Addy, A. L., Korst, H. H., White, R. A., and Walker, B. J., "A Study of Flow Separation in the Base Region and Its Effects During Powered Flight," AGARD CP 124, July 1973.

[4]Agrell, J., and White, R. A., "An Experimental Investigation of Supersonic Axisymmetric Flow over Boat tails Containing a Centered Propulsive Jet," Aeronautical Research Inst. of Sweden, Rept. FFA TN AU-913, Sept. 1974.

[5]Délery, J., and Sirieix, M., "Base Flows Behind Missiles," Short Course on *Missile Aerodynamics*, AGARD LS-98, March 1979.

[6]Korst, H. H., "A Theory for Base Pressure in Transonic and Supersonic Flow," *Journal of Applied Mechanics*, Vol. 23, No. 4, 1956, pp. 593–600.

[7]Addy, A. L., "Analysis of the Axisymmetric Base-Pressure and Base-Temperature Problem with Supersonic Interacting Freestream-Nozzle Flows Based on the Flow Model of Korst et al., Parts I, II and III," U.S. Army Missile Command, Rept. RD-TR-69-12, Redstone Arsenal, AL, July 1969.

[8]Carrière, P., Sirieix, M., and Délery, J., "Méthodes de calcul des écoulements turbulents décollés en supersonique (Computational Methods of Supersonic Turbulent Separated Flows)," *Progress in Aerospace Sciences*, Vol. 16, No. 4, 1975, pp. 385–429.

[9]Reijasse, P., Benay, R., Délery, J., and Lacau, R., "Missile and Projectile Base Flow Prediction by Multi-Component Methods," AIAA Paper 88-4380, Aug. 1988.

[10]Sahu, J., and Nietubicz, C. J., "Numerical Computation of Base-Flow for a Missile in the Presence of a Centered Jet," AIAA Paper 84-0527, Jan. 1984.

[11]Benay, R., and Servel, P., "Applications of a Navier–Stokes Code to the Calculation of Missile or Aircraft Afterbody Flows," *La Recherche Aérospatiale*, No. 6, 1995, pp. 405–426.

[12]Boutier, A., d'Humières, C., and Soulevant, D., "Three Dimensional Laser Velocimetry: a Review," *2nd International Symposium on Applications of Laser Anemometry to Fluid Mechanics*, Lisbon, Portugal, 1984.

[13]Dutton, J. C., Herrin, J. L., Molezzi, M. J., and Mathur, T., "Recent Progress on High-Speed Separated Base Flows," AIAA Paper 95-0472, Jan. 1995.

[14]Berner, C., "Measurements and Interpretation of 3-D High Speed Flows," *Proceedings of the 3rd International Conference on Laser Anemometry, Advances and Applications*, Swansea, Wales, UK, 1989.

[15]Lacau, R., Desnoyer, D., and Délery, J., "Analyse au vélocimètre laser de l'écoulement au culot en aval d'arrière-corps de missiles (An LDV Investigation of a Base Flow Past a Missile Afterbody)," *AGARD Symposium on Missile Aerodynamics*, Trondheim, Norway, Sept. 1982.

[16]Reijasse, P., and Délery, J., "Investigation of the Flow Past the ARIANE 5 Launcher Afterbody," *Journal of Spacecraft and Rockets*, Vol. 31, No. 2, 1994, pp. 208–214.

[17]Papamoshou, D., and Roshko, A., "The Compressible Turbulent Shear Layer: An Experimental Study," *Journal of Fluid Mechanics*, Vol. 197, Dec. 1988, pp. 453–477.

[18]Clemens, N. T., and Mungal, M. G., "Two- and Three-Dimensional Effects in the Supersonic Mixing Layer," AIAA Paper 90-1978, 1990.

[19]Samimy, N. D., and Elliott, G. S., "Effects of Compressibility on the Characteristics of Free Shear Layers," *AIAA Journal*, Vol. 28, No. 3, 1990, pp. 439–445.

[20]Goebel, S. G., and Dutton, J. C., "Velocity Measurements of Compressible, Turbulent Mixing Layers," AIAA Paper 90-0709, Jan. 1990.

[21]Jacquin, L., Mistral, S., Geffroy, P., and Cruaud, F., "Mixing of a Heated Supersonic Jet with a Supersonic Parallel Stream," *Advances in Turbulence V*, Springer–Verlag, Berlin, 1995, pp. 241–245.

[22]Reijasse, P., and Délery, J., "Problèmes de confluence en aval d'un arrière-corps. Etude de synthèse et description du montage expérimental (Flow Confluence Past an Afterbody. General Overview and Description of the Experimental Set-Up)," ONERA, Rept. 25/4361AY, Nov. 1993.

[23]Reijasse, P., and Corbel, B., "Etude expérimentale de la confluence d'écoulement supersonique en aval d'arrière-corps de révolution (Experimental Study of the Supersonic Flow Confluence Past an Axisymmetric Afterbody)," ONERA, Rept. 33/4361AY-AN, Dec. 1995.

[24]Délery, J., and Marvin, J., "Shock-Wave Boundary Layer Interactions," AGARDograph 280, Feb. 1986.

R. M. Cummings
Associate Editor